

Observation of superradiance in a phase fluctuating dipolar Bose-Einstein condensate

Bojeong Seo,^{1,*} Mingchen Huang,^{1,*} Ziting Chen,¹ Mithilesh K. Parit,¹ Yifei He,¹ Peng Chen,¹ and Gyu-Boong Jo^{1,2,3,†}

¹*Department of Physics, The Hong Kong University of Science and Technology, Clear Water Bay, Kowloon, Hong Kong, China*

²*IAS Center for Quantum Technologies, The Hong Kong University of Science and Technology, Kowloon, Hong Kong, China*

³*Microelectronics Thrust, The Hong Kong University of Science and Technology (Guangzhou), Guangzhou, China*

(Dated: January 3, 2024)

Despite the extensive study of matter-wave superradiance in a Bose-Einstein condensate (BEC) using its unique coherence property, the controllability of superradiant process has remained limited in the previous studies exploiting a phase-coherent condensate with isotropic contact interactions. Here, we combine tunable s-wave scattering with dipolar interactions in a BEC of ^{168}Er atoms wherein the asymmetry and threshold of superradiance are independently controlled. By changing the s-wave scattering length near the Feshbach resonance, we tune the superradiance threshold with increasing phase fluctuations. In contrast to collective light scattering from a condensate only with contact interactions, we observe an asymmetric superradiant peak in a dipolar BEC by changing the direction of external magnetic field. This results from the anisotropic excitation spectrum induced by the dipole-dipole interaction. Our observation is expected to bring forth unprecedented application of matter-wave optics leading to controlled emission of matter wave.

Collective light scattering [1], a cooperative emission process inducing directional scattered atoms, has been observed in various atomic systems ranging from thermal atoms [2, 3], degenerate Bose gases [4–12], free fermions [13] to atoms coupled to the cavity mode [14–16]. Among them, a Bose-Einstein condensate (BEC) has served as a promising platform for exploring a matter-wave superradiant process owing to its unique coherence property with [4–12] and without external light fields [17–20]. When the external light shines atoms in the condensate, collective scattering of light creates a quasiparticle in the form of recoiling atoms that interfere with condensate atoms at rest, leading to the generation of matter-wave grating that is further enhanced by subsequent light scattering. So far, however, it has been assumed in the previous studies that the condensate is phase-coherent and the superradiant gain of the process entails only external parameters such as the sample size and geometry. Furthermore, previous studies have remained in a weakly interacting regime, and neither the effect of strong s-wave interactions nor anisotropic dipolar interactions [21–23] has been addressed [24].

Here, we investigate matter wave superradiance of a dipolar BEC in an elongated trap, which combines tunable s-wave scattering with dipolar interactions, such that the superradiance process is significantly modified by phase fluctuations [25, 26] and anisotropic dispersion of the condensate [22, 23]. Such dipolar effects in quantum gases [27] have recently opened up a new regime where anisotropic dipole-dipole interactions play a crucial role for realizing new phases of matter, such as quantum droplets and supersolids [27]. In this work, dipolar interactions result in anisotropic dispersion of dipolar superfluid [22, 23], which allows us to control the asymmetry of superradiant peaks by changing the direction of

external magnetic field. Furthermore, by controlling the s-wave scattering length near the Feshbach resonance of ^{168}Er , we tune the superradiance threshold with increasing phase fluctuations [25, 26]. Our work demonstrates how the superradiance process can be controlled by the strength of s-wave scattering and the dipolar interaction.

When pump photons are scattered from a condensate, long-lived quasi-particles are excited leading to directional amplified Rayleigh scattering. The onset of the superradiant process is accounted for with the number of recoiling atoms N , following the rate equation $\dot{N} = (G - L)N$ where G is the gain of the superradiance and L is the loss term. A dipolar BEC of ^{168}Er offers a new opportunity for the unprecedented control of superradiance. First, with increasing s-wave scattering length, phase fluctuation shortens the coherence length [25, 26] and enhances the decay of the matter-wave grating resulting in the increase of L . Secondly, in contrast to alkali atoms with contact interactions, a dipolar BEC exhibits an anisotropic excitation spectrum due to the dipole-dipole interaction [21–23] resulting in anisotropic superradiant gain G being sensitive to the external magnetic field direction.

Our experiments begin with ^{168}Er BEC of approximately $1.8(2) \times 10^4$ atoms in the $|M_J = -6\rangle$ state [28, 29]. The atoms are trapped in the crossed optical dipole trap (ODT) consisting of two 1064 nm laser beams propagating along x-direction and y-direction with the beam waist of $w_{y-z} = 20 \mu\text{m}$ and $w_{x-z} = 45 \mu\text{m}$, respectively. To observe matter-wave superradiance, we gradually change the trap geometry over 45 ms, resulting in a quasi-1D trap with the trap frequency of $(\omega_x, \omega_y, \omega_z) = 2\pi \times (37, 445, 443)$ Hz and the maximum chemical potential of $\mu \simeq h \times 3.5$ kHz at $T \simeq 140(10)$ nK. During evaporative cooling, the magnetic field remains at 400 mG along

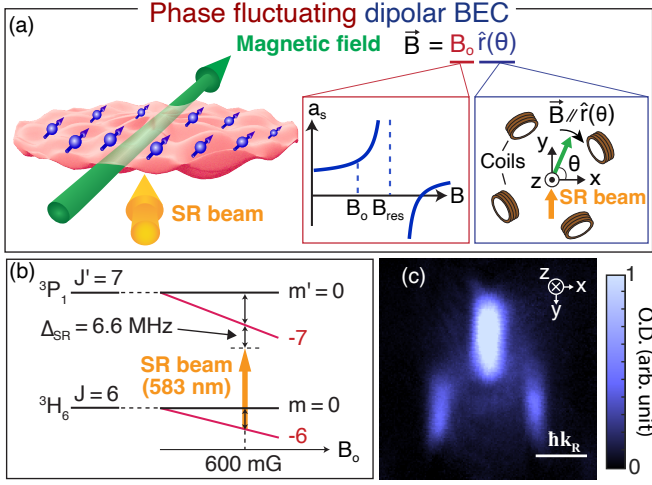


FIG. 1: **Superradiance from a phase fluctuating dipolar BEC of ^{168}Er** (a) An elongated condensate is exposed to the superradiance (SR) beam propagating along the $+y$ axis. The magnitude (B_0) and direction ($\hat{r}(\theta)$) of external magnetic field is independently controlled leading to tunable s-wave scattering and dipolar interactions. The pump beam is linearly polarized along the z-direction while the magnetic field is always on the xy-plane during the superradiance process. (b) Energy level diagram for relevant transitions are shown. We use a narrow-line transition ($4f^{12}6s^2(^3H_6) \rightarrow 4f^{12}(^3H_6)6s6p(^3P_1)$) with $\Gamma_{583}=2\pi \times 190$ kHz for superradiance. Orange arrow represents the $|J=6; m=-6\rangle \rightarrow |J'=7; m'=-7\rangle$ transition for a pump beam red-detuned by $\Delta_{SR}=7.767$ MHz (6.6 MHz) at 0 mG (600 mG) of external magnetic field. The external magnetic field changes between 300 mG and 912 mG during the experiment. (c) Time-of-flight image of superradiant dipolar BEC for $\theta = \pi/2$. After applying the pump beam, bi-directional recoiled atom clouds are generated. Here, $k_R = 2\pi/\lambda_{583}$ where $\lambda_{583}=583$ nm.

the y-direction. Before pulsing a pump light, we adjust the magnetic field to the target value at variable angle over t_{ramp} and switch off all ODT's within 60 μs . At this stage, phase fluctuation is controlled by the magnitude of bias magnetic field B_0 (near the Feshbach resonance) while the anisotropic dispersion relation is set by the field direction θ as described in Fig. 1.

To induce superradiant Rayleigh Scattering, an elongated condensate is illuminated with a single off-resonant 583 nm laser beam for 100 μs . The pump beam, linearly polarized along the z-direction (see Fig. 1), is about 100 times larger than the size of sample - with the Thomas-Fermi radius of 15 μm - to maintain the same optical intensity along the condensate. Additionally, the incident angle of the pump beam is perpendicular to the elongated axis to circumvent the unintended asymmetric superradiance [9]. Atomic momentum distribution after collective light scattering is recorded after a 16 ms of time-of-flight expansion using absorption imaging with a circularly polarized (σ^-) 401 nm broad-linewidth transition ($4f^{12}6s^2(^3H_6) \rightarrow 4f^{12}(^3H_6)6s6p(^1P_1)$) along the

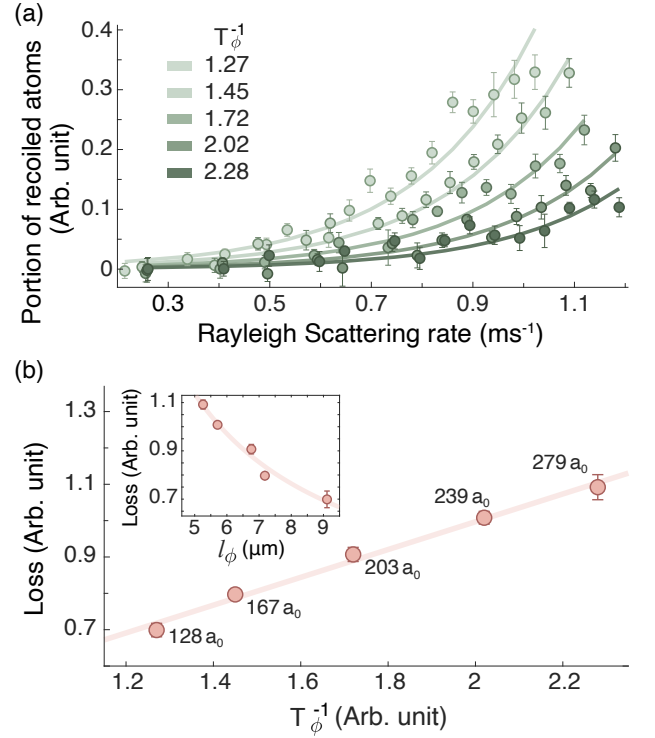


FIG. 2: **Control of superradiance threshold with the phase fluctuation** (a) Observation of portion of recoiled atoms versus the Rayleigh scattering rate R_{sc} for different phase fluctuation being proportional to T_ϕ^{-1} . To extract the threshold of Rayleigh scattering rate, corresponding to the loss term L , the data curve is fitted to the equation $N = Ae^{(R_{sc}-L)t_{pulse}}$ where $t_{pulse}=100\mu\text{s}$ and A is arbitrary coefficient. Error bars indicate the standard error of 20 consecutive measurements. (b) L is plotted against the T_ϕ^{-1} and a_s . The threshold of superradiance linearly increases with the amount of phase fluctuation in the condensate. Inset illustrated the decrease of the L against the increase of the coherence length l_ϕ . Error bars indicate 90% confidence interval of loss for the fitting in (a). Dashed lines are guides for eyes.

z-direction. With data from the absorption imaging, we quantify the number of recoiled atoms. The total number of recoiled atoms is denoted as $N = N_L + N_R$ where N_L and N_R are the number of atoms in left and right recoiled atom clouds, respectively (see Fig. 1).

In the first set of experiments, we test for the control of the loss term L by adjusting the phase coherence length of the condensate l_ϕ . When the condensate begins to interact with the superradiance pump photons, recoiling atoms form a matter-wave grating with the lifetime τ_c being proportional to $\tau_c \propto \frac{l_\phi}{v}$ where v and l_ϕ are the velocity of the recoiled atoms and the characteristic coherence length of the condensate, respectively. Here, the loss term increases with l_ϕ^{-1} as $L \propto 1/\tau_c \propto \frac{v}{l_\phi}$. For a condensate without phase fluctuations, the coherence length can be considered as the

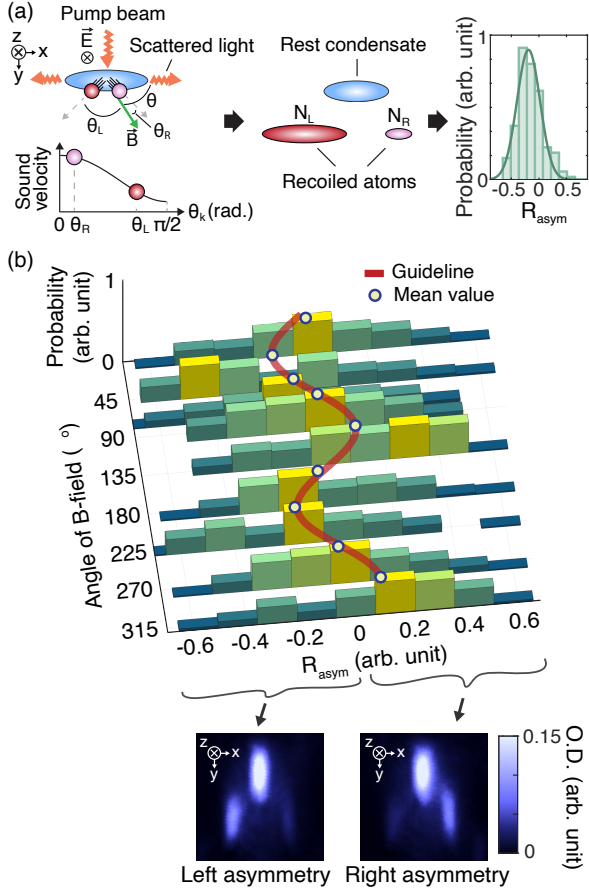


FIG. 3: Observation of asymmetric superradiant peaks. (a) When the magnetic field brakes the left-right symmetry, the atomic excitations propagating towards left and right superradiant peaks experience anisotropic dispersion resulting in the generation of asymmetric matter-wave gratings during the collective light scattering. By recording the number of recoiling atoms, we obtain the distribution of asymmetry ratio (R_{asym}) from the 170-300 consecutive measurements. (b) Histograms display the distribution of R_{asym} at a different angle θ of the magnetic field. The atomic momentum distribution after 16 ms time-of-flight shows left (right) asymmetric recoiling atoms corresponding to the negative (positive) mean value of R_{asym} . Yellow circles represent the mean values of the histograms. The red solid line was a guideline based on sinusoidal function.

Thomas-Fermi radius l of the condensate. With phase fluctuations, however, the coherence length is given by $l_\phi \simeq l(T_\phi/T)$ where T is the temperature and T_ϕ is the characteristic temperature of phase fluctuation defined as $T_\phi = 15(\hbar\omega_z)^2 N_{tot}/32\mu \propto a_s^{-2/5}$ with the reduced Planck constant \hbar . Here, μ is the chemical potential and the a_s is the scattering interaction length [25, 26]. Therefore, the loss term can be controlled by the scattering length as $L \propto T_\phi^{-1} \propto a_s^{2/5}$. In experiment, we exploit the Feshbach resonance at $B_{res} \simeq 912$ mG and control a_s from $128a_0$ to $279a_0$ with T_ϕ ranging from 100 nK to 50 nK

where a_0 is the Bohr radius.

To control the scattering length a_s , the magnetic field is changed from 400 mG to the target value within $t_{ramp} = 2.7$ ms right before the pump beam is switched on, while the field direction is kept along the x-axis (i.e. $\theta = 0$). For different magnetic fields, we tune the Rayleigh scattering rate upto 1.2 ms^{-1} based on the independent calibration (see supplementary note), which effectively control the gain term G . Subsequently, we record the portion of recoiled atoms against the change of Rayleigh scattering rate while we adjust the characteristic temperature of phase fluctuation (T_ϕ^{-1}) as shown in Fig. 2(a). Total recoiled atom number N exponentially grows as the Rayleigh scattering rate (or G) increases. Then, we extract the loss term L by fitting the initial rise of recoiling atom number with an exponential growth. We deduce the loss term from the measured threshold value. Fig. 2 (b) shows the change in the loss (L) for variable phase fluctuation characterized by T_ϕ^{-1} . The inset shows the decay of loss against the increase of coherence length.

In contrast to a BEC only with isotropic contact interactions, a dipolar BEC exhibits an anisotropic dispersion relation due to the dipole-dipole interaction [21–23]. The superradiant Rayleigh scattering is proportional to the square of the contrast of the matter wave interference between the condensate and the recoiling atoms. In a condensate without dipolar interactions, two matter-wave gratings, corresponding to opposite end-fire modes, are formed in a symmetric manner since the dispersion relation is isotropic with the constant sound velocity being insensitive to the angle between the external magnetic field and the propagation direction of atomic excitation. In other word, for the elongated condensate the gain G is the same for opposite directional emissions.

In a dipolar BEC, however, the number of recoiling atoms into opposite directions is sensitive to the orientation of magnetic field. By quantifying the contribution of dipole-dipole interaction a_{dd} with respect to the contact interactions as $\epsilon_{dd} = a_{dd}/a_s$ where $a_{dd} = 66.3 a_0$ in our system, the elementary Bogoliubov excitation spectrum $\hbar\omega(k)$ for a uniform density n is given as

$$\hbar\omega(k) = \sqrt{E(k)(E(k) + 2gn(1 + \epsilon_{dd}(3\cos^2\theta_k - 1))}$$

where $E(k) = \frac{\hbar^2 k^2}{2m}$ and θ_k is the angle between the external field and the atomic excitation propagating along \vec{k} , which reveals the anisotropy of the dispersion relation [21]. Here, $g = 4\pi\hbar^2 a_s/m$ with atomic mass m . With the sound velocity given as $c(\theta_k) = c_0\sqrt{1 + \epsilon_{dd}(3\cos^2\theta_k - 1)}$ where $c_0 = \sqrt{2gn}$, excitations propagating along the magnetic field direction (i.e. $\theta_k = 0$) are stiffer with a larger sound velocity of $c(0) = c_0\sqrt{1 + 2\epsilon_{dd}}$ than the one propagating in the perpendicular direction (i.e. $\theta_k = \pi/2$) with $c(\pi/2) = c_0\sqrt{1 - \epsilon_{dd}}$. In a confined system with inhomogeneous density, however, roton softening at finite momentum k is expected

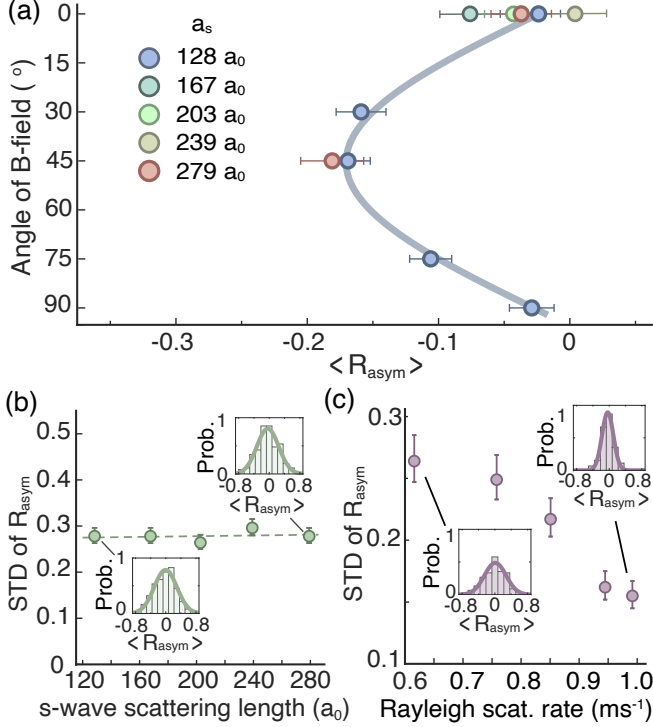


FIG. 4: **Insensitivity of asymmetric superradiance to the scattering length** (a) The asymmetry of superradiance peaks is insensitive to the scattering length a_s . The error bar is the standard error and the solid line is a guide for eyes. (b) The full distribution of asymmetry does not change with a_s within our experimental resolution. In this measurement, the magnetic field is changed within $t_{\text{ramp}}=0.5$ ms with phase fluctuations being negligible. (c) The distribution becomes narrower with the increasing Rayleigh scattering rate. In (b,c), the error bar represents the 1 sigma confidence interval of standard deviation of R_{asym} .

to change the collective excitation, but it is expected this effect is not significant in the current experiment with the small dipolar strength of $\epsilon_{dd} \lesssim 0.5$, revealing an anisotropic dispersion [30, 31].

In our experiment, the phase-matching condition in a given trap geometry allows scattered atoms to be only at 45° with respect to the x axis. When the magnetic field is oriented at $\theta=0^\circ$ or 90° , atomic excitations that involves opposite matter-wave gratings occur with the same strength as θ_k is $\pi/4$ for both cases. The effect of anisotropic dispersion becomes prominent when magnetic field is aligned to one of excitation directions (e.g. $\theta=45^\circ$ or 135°). At $\theta=45^\circ$, for example, the atomic excitation involving the right superradiant peak (N_R) undergoes stiffer dispersion with a larger excitation resonance frequency (for $\theta_k=0$) compared to the left peak (N_L). According to the f-sum rule, the excitation involving the increased resonance frequency (i.e. right peak) is relatively more suppressed than the left peak with a smaller resonance frequency [32] (see Fig. 3(a)).

To elucidate the effect of magnetic field direction on superradiance, we keep the Rayleigh scattering rate constant and therefore effectively the gain term of superradiance the same. In our experiment, the end-fire mode always occurs along the x direction regardless of magnetic field direction. In this case, the spontaneous emission strength along the x direction is sensitive to the quantization direction (i.e. external magnetic field) following the radiation pattern (see supplementary note). Therefore, we calibrate the intensity of the pump beam such that spontaneous emission along the longitudinal direction of the atom cloud remains constant for the different quantization directions. Furthermore, to avoid the shape change of condensate induced by the field direction we switch on a pump beam immediately after rapidly rotating the magnetic field in less than 0.5 ms.

In Fig. 3, we characterize a superradiant sample by recording an asymmetry of superradiant peaks. For each condition, we obtain around 170-300 data and plotted a histogram for an asymmetry ratio ($R_{\text{asym}} = \frac{N_R - N_L}{N_R + N_L}$) where N_R (N_L) represents the atom number of right (left) superradiant peak. When the left (right) atom cloud is dominant, the mean value of the histogram has a negative (positive) value (see yellow circles in Fig. 3).

It is interesting to notice that the anisotropic dispersion relation depends only on the absolute magnitude of dipolar interaction a_{dd} - not the relative strength ϵ_{dd} - as shown in sound velocity $c(\theta_k) = \sqrt{gn/m + \frac{4\pi\hbar^2 na_{dd}}{m^2}(3\cos^2\theta_k - 1)}$. To test for the insensitivity of asymmetric superradiance to the chemical potential, we monitor the asymmetry of superradiant peaks at different scattering lengths. In Fig. 4(a), the mean value of R_{asym} does not change with increasing a_s confirming our understanding. In this case, the full distribution of R_{asym} is also insensitive to a_s as shown by solid green circles in Fig. 4(b).

Finally, for experimentally observed asymmetry R_{asym} of around 100-150 consecutive measurements we find a finite width of the R_{asym} distribution even when the superradiance process is symmetric with the mean value of R_{asym} close to zero. We attribute this partly to the finite size of the condensate with an aspect ratio of 12, which results in possible tilting of the end fire mode by $\pm 5^\circ$. This may introduce the uncertainty of the direction of recoiling atoms, $\delta\theta_k \sim 0.055\pi$. We also find that the distribution becomes narrower with the increasing Rayleigh scattering rate in Fig. 4(c), which suggests asymmetric superradiance occurs at the early stage of the process.

In conclusion, we have explored a superradiant process in a dipolar BEC with phase fluctuations highlighting versatile tools for controlling a matter-wave superradiance process. The anisotropic dispersion allows us to control asymmetric superradiant peaks by changing the direction of external magnetic field. Furthermore, we demonstrate how to tune the superradiance threshold

by adjusting coherence property of BEC. In the future, it will be interesting to investigate a superradiant process in an oblate dipolar condensate [31]. It is then anticipated that the direction of recoiling atoms may be controlled by the external magnetic field direction. Another interesting future direction is to explore collective light scattering in dipolar fermions [33, 34] or dipolar molecules [35].

Acknowledgements We thank Hui Zhai for fruitful discussions. We acknowledge support from the RGC through 16304918, 16308118, 16306119, 16302420, 16302821, 16306321 C6005-17G, C6009-20G and RFS2122-6S04. This work is also supported by the Guangdong-Hong Kong Joint Laboratory and the Hari Harilela foundation.

* Theres authors contributed equally.

† Electronic address: gbjo@ust.hk

- [1] R. H. Dicke, *Physical Review* **93**, 99 (1954).
- [2] M. Gross and S. Haroche, *Physics Reports* **93**, 301 (1982).
- [3] Y. Yoshikawa, Y. Torii and T. Kuga, *Physical Review Letters* **94**, 083602 (2005).
- [4] S. Inouye, A. Chikkatur, D. M. Stamper-Kurn, J. Stenger, D. Pritchard and W. Ketterle, *Science* **285**, 571 (1999).
- [5] J. Stenger, S. Inouye, D. Stamper-Kurn, A. Chikkatur, D. Pritchard and W. Ketterle, *Applied Physics B* **69**, 347 (1999).
- [6] S. Inouye, T. Pfau, S. Gupta, A. P. Chikkatur, A. Gorlitz, D. E. Pritchard and W. Ketterle, *Nature* **402**, 641 (1999).
- [7] L. Fallani, C. Fort, N. Piovella, M. Cola, F. S. Cataliotti, M. Inguscio and R. Bonifacio, *Physical Review A* **71**, 033612 (2005).
- [8] L. Deng, E. W. Hagley, Q. Cao, X. Wang, X. Luo, R. Wang, M. G. Payne, F. Yang, X. Zhou, X. Chen et al., *Physical Review Letters* **105**, 220404 (2010).
- [9] B. Lu, X. Zhou, T. Vogt, Z. Fang and X. Chen, *Physical Review A* **83**, 033620 (2011).
- [10] N. S. Kampel, A. Griesmaier, M. P. H. Steenstrup, F. Kaminski, E. S. Polzik and J. H. Muller, *Physical review letters* **108**, 090401 (2011).
- [11] R. Lopes, A. Imanaliev, M. Bonneau, J. Ruaudel, M. Cheneau, D. Boiron and C. I. Westbrook, *Physical Review A* **90**, 013615 (2014).
- [12] I. Dimitrova, W. Lunden, J. Amato-Grill, N. Jepsen, Y. Yu, M. Messer, T. Rigaldo, G. Puentes, D. Weld and W. Ketterle, *Physical Review A* **96**, 051603 (2017).
- [13] P. Wang, L. Deng, E. W. Hagley, Z. Fu, S. Chai and J. Zhang, *Physical Review Letters* **106**, 210401 (2010).
- [14] S. Slama, S. Bux, G. Krenz, C. Zimmermann and P. W. Courteille, *Physical Review Letters* **98**, 053603 (2007).
- [15] K. Baumann, C. Guerlin, F. Brennecke and T. Esslinger, *Nature* **464**, 1301 (2010).
- [16] H. Kessler, J. Klinder, M. Wolke and A. Hemmerich, *Physical Review Letters* **113**, 070404 (2014).
- [17] L. W. Clark, A. Gaj, L. Feng and C. Chin, *Nature* **551**, 356 (2017).
- [18] H. Fu, L. Feng, B. M. Anderson, L. W. Clark, J. Hu, J. W. Andrade, C. Chin and K. Levin, *Physical Review Letters* **121**, 243001 (2018).
- [19] Z. Wu and H. Zhai, *Physical Review A* **99**, 063624 (2019).
- [20] K. Kim, J. Hur, S. Huh, S. Choi and J.-y. Choi, *Physical Review Letters* **127**, 043401 (2021).
- [21] T. Lahaye, C. Menotti, L. Santos, M. Lewenstein and T. Pfau, *Reports on Progress in Physics* **72**, 126401 (2009).
- [22] G. Bismut, B. Laburthe-Tolra, E. Marechal, P. Pedri, O. Gorceix and L. Vernac, *Physical Review Letters* **109**, 155302 (2012).
- [23] M. Wenzel, F. Bottcher, J.-N. Schmidt, M. Eisenmann, T. Langen, T. Pfau and I. Ferrier-Barbut, *Physical Review Letters* **121**, 030401 (2018).
- [24] M. Gross and S. Haroche, *Phys. Rep.* **93**, **301** (1982).
- [25] D. S. Petrov, G. V. Shlyapnikov and J. T. M. Walraven, *Physical Review Letters* **87**, 050404 (2001).
- [26] S. Dettmer, D. Hellweg, P. Ryytty, J. J. Arlt, W. Ertmer, K. Sengstock, D. S. Petrov, G. V. Shlyapnikov, H. Kreutzmann, L. Santos et al., *Physical Review Letters* **87**, 160406 (2001).
- [27] L. Chomaz, I. Ferrier-Barbut, F. Ferlaino, B. Laburthe-Tolra, B. L. Lev and T. Pfau, *arXiv:2201.02672*, (2022).
- [28] B. Seo, P. Chen, Z. Chen, W. Yuan, M. Huang, S. Du and G.-B. Jo, *Physical Review A* **102**, 013319 (2020).
- [29] B. Seo, Z. Chen, M. Huang, M. K. Parit, Y. He, P. Chen and G.-B. Jo, *Journal of Korean Physical Society* **82** 901 (2023).
- [30] R. M. Wilson, S. Ronen and J. L. Bohn, *Physical Review Letters* **104**, 094501 (2010).
- [31] C. Ticknor, R. M. Wilson and J. L. Bohn, *Physical Review Letters* **106**, 065301 (2011).
- [32] P. Nozieres, *The Theory of Quantum Liquids* (1990).
- [33] M. Lu, N. Q. Burdick and B. L. Lev, *Physical Review Letters* **108**, 215301 (2012).
- [34] K. Aikawa, A. Frisch, M. Mark, S. Baier, R. Grimm and F. Ferlaino, *Physical Review Letters* **112**, 010404 (2014).
- [35] K. K. Ni, S. Ospelkaus, M. H. G. d. Miranda, A. Pe'er, B. Neyenhuis, J. J. Zirbel, S. Kotochigova, P. S. Julienne, D. S. Jin and J. Ye, *Science* **322**, 231 (2008-10).

Supplementary Note

Calibration of Rayleigh scattering rate In our experiment, the Rayleigh scattering rate has been independently calibrated at different magnetic field. Considering Lande g-factors for $|J' = 7; m' = -7\rangle$ and $|J = 6; m = -6\rangle$ are $g_e = -11.71$ MHz/G and $g_g = -9.77$ MHz/G, respectively, we compensate the change of detuning δ induced by the Zeeman shift by adjusting the intensity I of the pump beam following the relation

$$R_{scatt} = \frac{\Gamma_{583}}{2} \frac{\Omega_R^2/2}{\delta^2 + \Omega_R^2/2 + \Gamma_{583}^2/4}$$

with the Rabi frequency $\Omega_R = \Gamma_{583} \sqrt{\frac{I}{2I_{sat}}}$. As an example, we select 300 mG and 400 mG in Fig. S1 where the phase fluctuation can be avoided with the small scattering length, and monitor the number of recoiling atoms as a function of Rayleigh scattering rate.

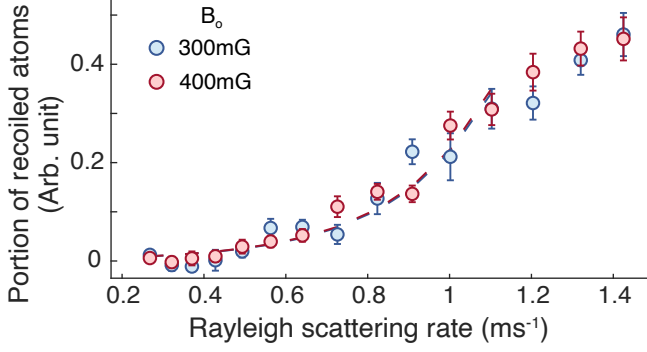


FIG. S1: **Rayleigh scattering rate calibration.** The Rayleigh scattering rate is independently controlled at different magnetic fields. For example, we calibrate the superradiance at 300 mG and 400 mG, where a_s are almost the same. The dashed lines are a guideline. The error bar is the standard deviation.

Calibration of effective pumping intensity Radiation from an atom has an angular dependence on a quantization axis. Therefore, the Rayleigh scattering rate changes while we rotate the external magnetic field during experiments. Additionally, only radiation along the longitudinal direction of the atom cloud is amplified by the gain medium and contributes the superradiance. Therefore, we calibrate the intensity of the pump beam such that spontaneous emission along the longitudinal direction of the atom cloud remains con-

stant for the different quantization directions. Since the superradiance process involves σ -transitions, the angular distribution of emission spectrum I_{eff} is given as $I_{eff}(\alpha) = I(1 + \cos^2 \alpha)/2$ where I is the intensity of the pump beam and α is an angle of the emission direction with respect to the quantization axis.

To observe asymmetric superradiance induced by the dipole-dipole interaction, we keep the constant scattering rate into the end-fire mode (i.e. I_{eff}) by using variable pump intensity $I(\theta)$ as $I(\theta) = 2I_{eff}/(1 + \cos^2 \theta)$ where the magnetic field has an angle θ with respect to the x axis. Fig. S2 shows the angular dependence of the required pump beam intensity at different angle of magnetic field.

Rotation of magnetic field Bias magnetic field was generated by three pairs of Helmholtz coils perpendicular to each other in Fig. 1. To rotate the direction of the magnetic field, we tuned currents in coils within 500 μ s. Due to the dipole-dipole interaction, the shape of dipolar condensates could be changed when the direction of the magnetic field was tuned. Moreover, the cloud shape change affects the gain of the superradiance. Hence, we prevented the cloud shape change by sending a pump beam immediately after rapidly rotating the magnetic field in less than 0.5 ms.

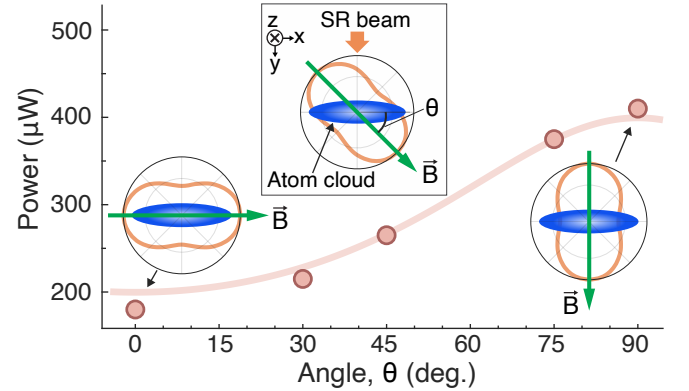


FIG. S2: **Calibration of effective pumping intensity** When collective lights scattering occurs, we keep the emission rate along the x-direction constant as the magnetic field rotates. The required pump beam intensity scales as $1/(1 + \cos^2 \theta)$ as described by a solid curve. Ellipses and dumbbells in insets are atom condensates and radiation patterns, respectively at 0° , 45° , and 90° . Here, θ is an angle of magnetic field (green arrow) with respect to the longitudinal direction of the atom cloud.